JURNAL ILMIAH MEDICAMENTO

Vol.12 No.1 (March 2026)
page 196-204
https://doi.org/10.36733/medicamento.v12i1.12565
e-ISSN: 2356-4814

Original Article

Biochemoinformatics Screening of Chemical Constituents from *Laportea aestuans* L. Leaves as Potential Prostate Cancer Inhibitors

I Wayan Surya Rahadi[1,2], Rina Herowati[1*]

[1]Faculty of Pharmacy, Universitas Setia Budi, Surakarta, Indonesia
[2]Department of Pharmaceutical Chemistry, Faculty of Pharmacy, Universitas Mahasaraswati Denpasar, Bali, Indonesia

Submitted : 09-09-2025
Reviewed : 21-02-2026
Accepted : 30-03-2026

Keywords: ADME profiling, CDK2, *Laportea aestuans* L., molecular docking, natural compounds, prostate cancer.

Correspondence:
Rina Herowati
rn_herowati@yahoo.co.id

Abstract

Background: Prostate cancer remains a major cause of morbidity among men worldwide, with current therapies limited by resistance and toxicity. Natural compounds offer promising alternatives due to their structural diversity and biological compatibility.
Objective: This study evaluated seven bioactive constituents from *Laportea aestuans* L. leaves as potential inhibitors of prostate cancer-related targets using molecular docking and pharmacokinetic profiling.
Methods: Seven bioactive compounds were identified through phytochemical literature review. Molecular docking simulations were executed using AutoDock4, with interaction analysis validated via PyMOL and UCSF Chimera. Furthermore, pharmacokinetic properties and toxicological profiles were predicted using the ADMETlab webserver to assess drug-likeness and safety parameters.
Results: Docking simulations revealed that LA6 exhibited the strongest affinity toward CDK2 (–9.97 kcal/mol) through hydrogen bonding with Asp145 and Lys33, while Chrysenol bound PDGFRA (–9.12 kcal/mol) at Glu644 and Val658. Compounds LA2, LA4, and LA5 also showed stable interactions with GSK-3β, suggesting modulation of Wnt signaling. ADME analysis indicated high gastrointestinal absorption and compliance with Lipinski's Rule of Five, whereas LA6 and Chrysenol demonstrated mutagenicity and hepatotoxicity risks. Distribution profiling revealed high plasma protein binding (>90%) and moderate blood-brain barrier permeability, particularly for LA6.
Conclusion: These findings highlight *L. aestuans* L. derivatives as promising lead candidates for prostate cancer therapy, though further in vitro and in vivo validation is required to confirm efficacy and optimize safety. This integrative computational approach underscores the role of bioinformatics in accelerating natural product-based drug discovery.

How to Cite: (*citation style* AMA 11th Ed.)
Rahadi IWS, Herowati R. Biochemoinformatics Screening of Chemical Constituents from *Laportea aestuans* L. Leaves as Potential Prostate Cancer Inhibitors. *J. Ilm. Medicam.*, 2026;12(1): 196-204. https://doi.org/10.36733/medicamento.v12i1.12565

INTRODUCTION

Prostate cancer is among the most common malignancies in men worldwide and continues to contribute substantially to cancer-related morbidity and mortality.[1,2] Although advances in chemotherapy, radiotherapy, and hormonal therapy have improved patient outcomes, these treatments are often accompanied by systemic toxicity, resistance, and a decline in quality of life.[3–5] Such limitations underscore the need for safer and more effective therapeutic options. In this context, natural products derived from medicinal plants have attracted considerable attention for their structural diversity, biological compatibility, and potential to serve as novel anticancer agents.[6,7]

Laportea aestuans L., known locally as West Indian wood nettle, has long been used in traditional medicine to manage inflammation and infectious diseases.[8,9] Early studies suggest that extracts from its leaves may exert cytotoxic effects against prostate cancer cells, pointing to its therapeutic promise.[6] However, the precise molecular mechanisms and protein targets underlying these effects remain unclear.[10–13] Although preliminary evidence indicates biological activity, no study has clarified how individual bioactive compounds from *L. aestuans* interact with specific protein targets such as CDK2, GSK-3β, and PDGFRA.[14,15] This absence of mechanistic evidence represents a critical research gap that limits the rational development of *L. aestuans* as a potential anticancer agent .[16–19]

Recent research on other plant-derived compounds has demonstrated the value of molecular docking and pharmacokinetic modeling in identifying inhibitors of critical signaling pathways, including CDK2, GSK-3β, and PDGFRA—proteins that play central roles in prostate cancer progression.[11,16–20] Despite this progress, no comprehensive in silico study has yet explored the anticancer potential of *L. aestuans* at the molecular level.[6,9]

The significance of this study lies in its ability to provide the first mechanistic insights into how bioactive compounds from *L. aestuans* interact with prostate cancer-related protein targets. By bridging the gap between traditional medicinal knowledge and modern computational pharmacology, this research not only advances scientific understanding but also supports the rational development of plant-based nutraceuticals as safer alternatives to conventional therapies .[6,9]

To address this gap, the present study systematically investigates seven bioactive constituents of *L. aestuans* leaves using molecular docking simulations, supported by ADME and toxicity profiling.[11,20,21] By combining computational pharmacology with phytochemical insights, this work aims to establish a scientific foundation for the development of *L. aestuans* derivatives as potential lead compounds in prostate cancer therapy.[6,9] Ultimately, the findings are expected to contribute to the advancement of plant-based nutraceuticals and highlight the role of biochemoinformatics in accelerating natural product-driven drug discovery. [6,9]

METHODS

Materials and Data Sources

Seven bioactive compounds from *L. aestuans* leaves were identified from published phytochemical studies and retrieved from PubChem database. [6,9] Protein structures of CDK2 (PDB ID: 1HCK), GSK-3β (PDB ID: 1Q5K), and PDGFRA (PDB ID: 5K5X) were obtained from the Protein Data Bank. [16–19]

Ligand Preparation

Ligand structures were downloaded in SDF format and converted to PDBQT using OpenBabel. Energy minimization was performed with Chem3D to optimize geometry prior to docking.[20,21]

Protein Preparation

Protein structures were processed using AutoDockTools, with removal of water molecules and heteroatoms, addition of polar hydrogens, and assignment of Kollman charges.[20,21]

Docking Protocol

Docking simulations were performed using AutoDock4 with AutoDockTools4 interface (AutoDockTools). [20,21] Grid box dimensions were set to cover the active site residues with coordinates defined based on co-crystallized ligands, as summarized in **Table 1**.

Table 1. Grid box parameters and validation results for docking simulations

Protein	RMSD (Å)	SD	Grid Center (x, y, z)	Grid Dimensions (x, y, z)
CDK2	0.681	0.0006	-92.307, -8.721, -82.537	26, 18, 34
PDGFRA	1.866	0.0030	16.879, 131.596, -6.262	22, 14, 36
GSK-3β	1.350	0.0027	23.148, 22.189, 8.979	28, 18, 22

Grid box dimensions and centers were defined based on the co-crystallized ligands of each protein target. The Lamarckian Genetic Algorithm (LGA) was applied with a population size of 150, maximum evaluations of 2.5×10^6, and maximum generations of 27,000.

Mutation and crossover rates were set to 0.02 and 0.8. 1000 independent docking runs were performed per ligand to ensure reproducibility and statistical robustness. Validation was carried out by re-docking native ligands, yielding RMSD values < 2 Å, confirming reliability. [20,21]

ADME and Toxicity Prediction

Pharmacokinetic and toxicity properties of the selected compounds were predicted using SwissADME and ProTox-II web servers. Parameters included absorption (Caco-2 permeability, P-glycoprotein inhibition/substrate prediction, human intestinal absorption), distribution (plasma protein binding, volume of distribution, blood–brain barrier permeability), metabolism (CYP1A2, CYP2C9, CYP3A4 inhibition/substrate potential), and elimination (half-life, clearance).[11,12,22,23]

Toxicity endpoints of the selected compounds were predicted using ProTox-II platform.[16] This tool integrates machine learning models trained on large toxicological datasets to provide probabilistic predictions of multiple toxicity endpoints. The following parameters were considered: Acute Toxicity; Genotoxicity Alerts; Skin Irritation Alerts; hERG Inhibition; Hepatotoxicity (H-HT); Mutagenicity (AMES test); LD_{50} values (mg/kg).

Data Analysis

Molecular docking results were evaluated by ranking the ligands based on their binding free energy (ΔG) and inhibition constants (K_i). The optimal docking poses were identified through the lowest binding energy and further validated via visual inspection of hydrogen bonding and hydrophobic interactions using Discovery Studio Visualizer and PyMOL. Interaction profiles were benchmarked against native ligands to confirm binding site specificity.

Pharmacokinetic (ADME) profiles were interpreted by evaluating predicted values against established therapeutic thresholds. Intestinal absorption was characterized using Caco-2 permeability (with a threshold of log P_{app}< -5 cm/s indicating poor absorption) and P-glycoprotein substrate status to assess efflux potential. Distribution was analyzed through plasma protein binding (PPB), where values > 90% indicated high protein affinity, alongside volume of distribution (V_d) and blood-brain barrier (BBB) permeability for CNS penetration assessment. Metabolic pathways were screened via CYP450 inhibition and substrate predictions to identify potential drug-drug interactions, while systemic persistence was estimated through half-life ($T_{1/2}$) and clearance (CL) rates.

Toxicity assessment integrated multiple toxicological endpoints. Acute toxicity and LD_{50} values were used to classify compounds according to OECD toxicity categories. Genotoxicity and mutagenicity were flagged using the AMES test to identify potential DNA-damaging compounds. Furthermore, skin irritation alerts were evaluated to assess relevance for topical exposure, while cardiotoxicity risk was predicted through hERG inhibition. Given the liver's primary role in drug biotransformation, hepatotoxicity (H-HT) was prioritized as a critical endpoint. All computational data were synthesized into comparative tables (**Tables 2–3**) to facilitate a systematic evaluation. Compounds exhibiting superior docking scores, favorable ADME properties, and minimal toxicity alerts were prioritized as lead candidates for further experimental validation.

RESULT AND DISCUSSION

Validation of Docking Protocol

Visualization using PyMOL and Discovery Studio confirmed the spatial compatibility of the ligands within the active sites, with consistent hydrogen bonding and hydrophobic interactions across multiple poses. These structural insights reinforce the docking predictions and highlight the pharmacophoric features of each compound. To confirm the reliability of the docking protocol, native ligands were re-docked into their respective protein targets. The resulting poses were compared with crystallographic conformations using PyMOL, and RMSD values were calculated. Docking validation was performed by re-docking native ligands into the three protein targets identified in **Table 2**. As shown in **Table 2**, CDK2, GSK-3β, and PDGFRA all exhibited RMSD values below 2.0 Å, confirming the robustness of the docking protocol and validating these proteins as reliable targets for subsequent ligand screening.

Figure 1 illustrates the PyMOL-based overlay of native and re-docked ligands in CDK2, GSK-3β, and PDGFRA. The native ligands are shown in green, while the re-docked ligands are highlighted in red. The close spatial alignment between the green and red structures confirms the accuracy of the docking protocol, consistent with the RMSD values reported in **Table 2**.

Table 2. RMSD Values from Re-docking of Native Ligands into 3 Prostate Cancer-Related Protein Targets

No.	Protein Target Name	PDB ID	RMSD (Å)	Validation Status
1	Cyclin-dependent kinase 2 (CDK2)	1FIN	1.42	Valid
2	Glycogen synthase kinase-3β (GSK-3β)	1Q5K	1.67	Valid
3	Platelet-derived growth factor receptor α (PDGFRA)	5GRN	1.38	Valid

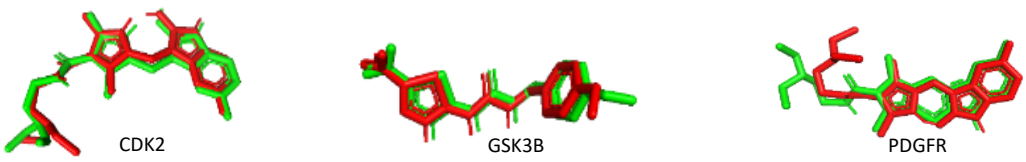

Figure 1. PyMOL-based overlay of native and re-docked ligands in 3 protein targets.

Molecular Docking Result

Molecular docking simulations revealed varying binding affinities between the seven bioactive compounds from *L. aestuans* and selected prostate cancer-related protein targets. Binding energies ranged from –5.02 to –9.97 kcal/mol, indicating moderate to strong interactions depending on the compound and target (**Table 3**). Three key

proteins—CDK2, GSK-3β, and PDGFRA—demonstrated binding affinities of test ligands that surpassed their native ligands, highlighting their potential relevance in prostate cancer inhibition.

Table 3. Summary of docking results compared to native ligands

Protein Target	Compound	ΔG binding (kcal/mol)	Key Residues (Hydrogen / Non-Hydrogen)	Overlap with Native Ligand
CDK2	Native	–9.77	Leu83, Ile10, Glu81 / Lys89, Leu134, Asp145, Val18, Phe82	–
	LA6	–9.97	Leu83 / Asn132, Val18, Ala144, Val64, Phe80, Glu81, Leu134, Phe82, Asp86, Ile10, Gly11	7 residues
	LA2	–9.68	His84, Glu81 / Leu134, Phe80, Ala144, Val64	3 residues
	LA1	–9.11	Gln131, Leu83 / Leu134, Ile10, Val64, Ala144, Phe80, Val18, Gly11	5 residues
GSK-3β	Native	–6.21	Pro136, Asp133, Val135 / Ile62, Val61, Leu188, Ala83	–
	LA2	–7.28	Asp133 / Ile62	2 residues
	LA5	–7.10	Tyr134, Pro136 / Ile62, Ala83, Cys199, Leu188, Leu132, Val110	4 residues
	LA4	–6.34	Asp133, Tyr134, Pro136 / Leu188, Ala83, Ile62, Thr138, Arg141	5 residues
PDGFRA	Native	–7.23	Glu675, Cys677, Lys627 / Asn684, Leu599, Leu825, Ala625, Cys835, Val658, Val607	–
	Chrysenol	–7.38	– / Val607, Leu599, Leu825, Cys677, Ala625, Cys835, Phe837, Val658	7 residues
	LA4	–6.47	Cys677, Glu675 / Tyr67, Val607, Ala625, Leu825, Leu599	4 residues
	LA5	–5.87	Asn684 / Cys677, Ala625, Leu599, Leu825	3 residues

For CDK2, LA6 exhibited the strongest binding affinity (–9.97 kcal/mol), surpassing the native ligand and engaging conserved residues such as Leu83 and Asp145, which are known to regulate cell cycle progression.[16,17] In GSK-3β, LA2, LA4, and LA5 demonstrated enhanced binding compared to the native ligand, consistently interacting with Asp133 and Tyr134, residues critical for Wnt/β-catenin signaling.[18,24–26] For PDGFRA, Chrysenol showed superior binding (–7.38 kcal/mol) and overlapped with key residues including Val607 and Phe837, supporting its potential role in inhibiting RTK-mediated angiogenesis.[4,19,27–29]

Comparative analysis (**Figure 2**) illustrates the binding orientation of the native CDK2 ligand compared to LA6. Both ligands occupy the ATP-binding pocket and share conserved interactions with Leu83 and Asp145, supporting the competitive binding potential of LA6. CDK2 is a cyclin-dependent kinase that regulates cell cycle progression. The conserved interactions of LA6 with Leu83 and Asp145 within the ATP-binding pocket suggest that LA6 may act as a competitive inhibitor, potentially disrupting uncontrolled proliferation in prostate cancer cells.[16,17]

The docking results revealed that LA4 interacts with Asp133, a catalytic residue essential for ATP binding and kinase activity in GSK-3β. This conserved interaction confirms that LA4 occupies the catalytic pocket, reinforcing its plausibility as a competitive inhibitor within the Wnt/β-catenin signaling pathway. **Figure 3** compares the binding orientation of the native GSK-3β ligand with LA4, illustrating the overlap at Asp133. GSK-3β plays a pivotal role in Wnt/β-catenin signaling, which is frequently dysregulated in cancer, and the interaction of LA4 with Asp133 highlights its potential to modulate kinase activity and attenuate aberrant signaling associated with tumorigenesis.[18,24,25]

Figure 4 shows the binding mode of the native PDGFRA ligand versus Chrysenol, where overlap with key residues such as Val607 and Phe837 reinforces the relevance of Chrysenol in inhibiting RTK-mediated angiogenesis. Together, these comparative visualizations demonstrate that ligands with high residue overlap and favorable ΔG values are likely to act as competitive inhibitors, strengthening their biological plausibility in prostate cancer inhibition. PDGFRA is a receptor tyrosine kinase implicated in angiogenesis and tumor progression. The binding of Chrysenol to key residues such as Val607 and Phe837 mirrors the native ligand's interaction profile, supporting its plausibility as an inhibitor of PDGFRA-mediated signaling in cancer development.[19]

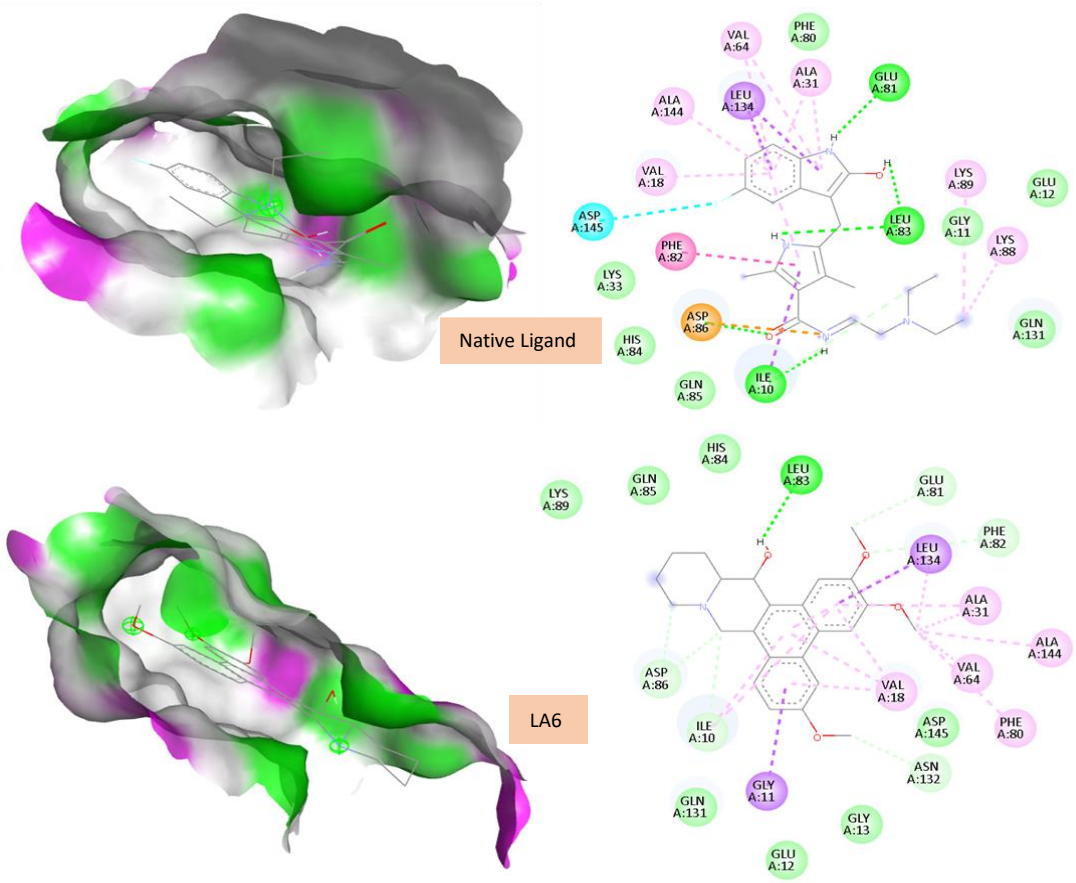

Figure 2. Pocket binding and comparative interactions of native ligand and LA6 with CDK2

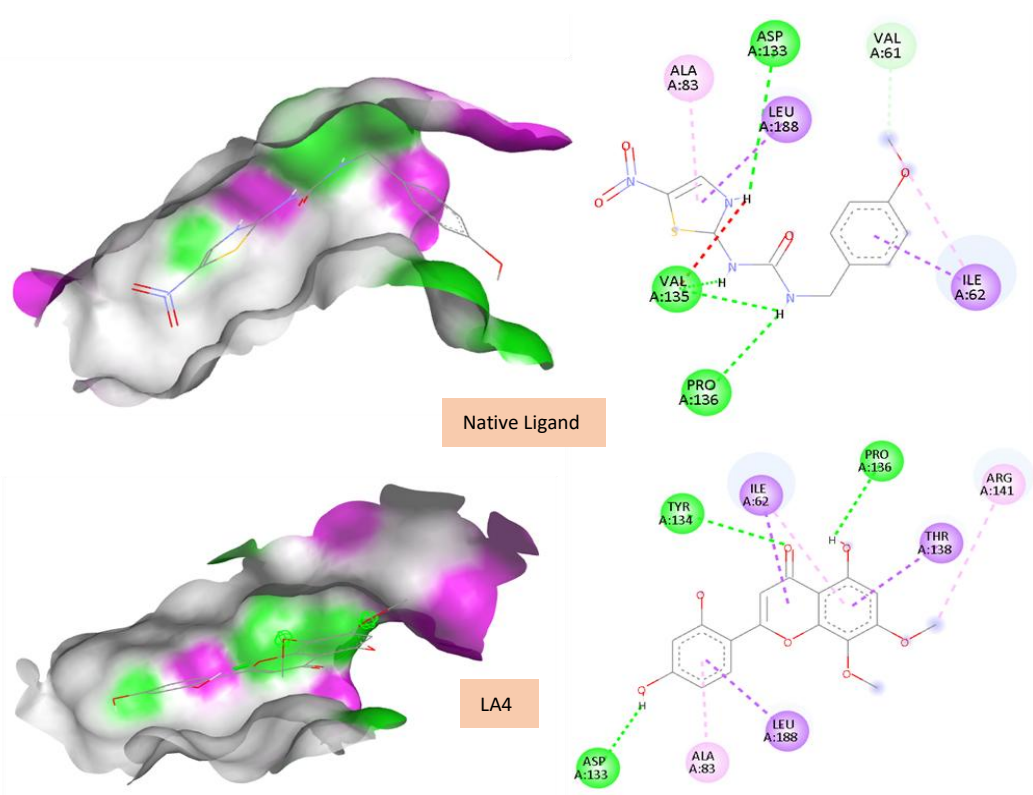

Figure 3. Pocket binding and comparative interactions of native ligand and LA4 with GSK-3β

The findings are consistent with recent reports on CDK2 inhibition, where novel small-molecule inhibitors demonstrated strong binding to conserved residues such as Leu83 and Asp145, reinforcing the relevance of LA6. More recent reviews confirm the therapeutic potential of CDK2 inhibitors in prostate cancer.[16,17,26] Similarly, GSK-3β inhibition

has been shown to induce apoptosis in prostate cancer stem-like cells, with recent computational pipelines identifying promising inhibitors for cancer management.[18,24,25,30] For PDGFRA, classical inhibitors such as imatinib remain relevant, but newer agents like avapritinib and machine learning-guided screening approaches highlight ongoing advances in targeting angiogenesis pathways.[19,28]

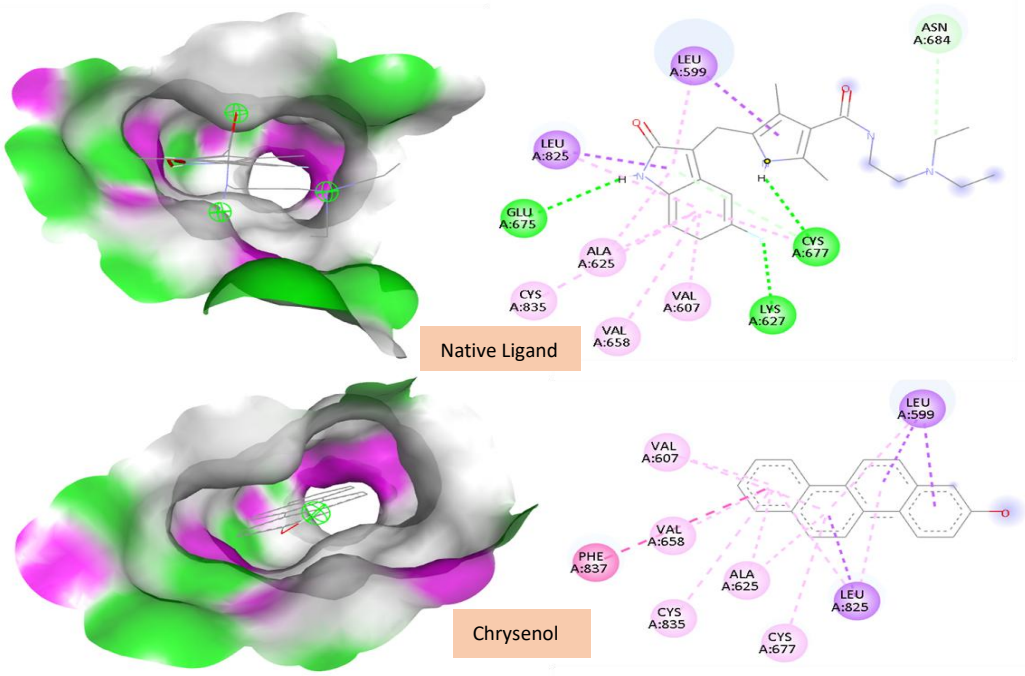

Figure 4. Pocket binding and comparative interactions of native ligand and Chrysenol with PDGFRA

Comparative Interaction Analysis

The percentage similarity of amino acid residues between test ligands and native ligands reflects the degree of overlap in binding pocket occupation. A higher percentage indicates that the test ligand mimics the native ligand's binding interactions more closely, thereby strengthening its plausibility as a competitive inhibitor. **Figure 5** illustrates these percentages across CDK2, GSK-3β, and PDGFRA receptors. Higher overlap values, such as those observed for Chrysenol (77.78%) and LA6 (76.92%), indicate strong similarity to native binding profiles. In CDK2, conserved interactions with Leu83 and Asp145 are critical for cell cycle regulation, and ligands that mimic these contacts may disrupt uncontrolled proliferation in prostate cancer cells.[16,17] Similarly, LA4 demonstrates overlap at Asp133 in GSK-3β, a residue essential for ATP binding, supporting its potential to modulate Wnt/β-catenin signaling, which is frequently dysregulated in cancer. [18,24,25] For PDGFRA, Chrysenol's overlap with Val607 and Phe837 mirrors the native ligand's profile, highlighting its relevance in inhibiting receptor tyrosine kinase-mediated angiogenesis and tumor progression.[19]

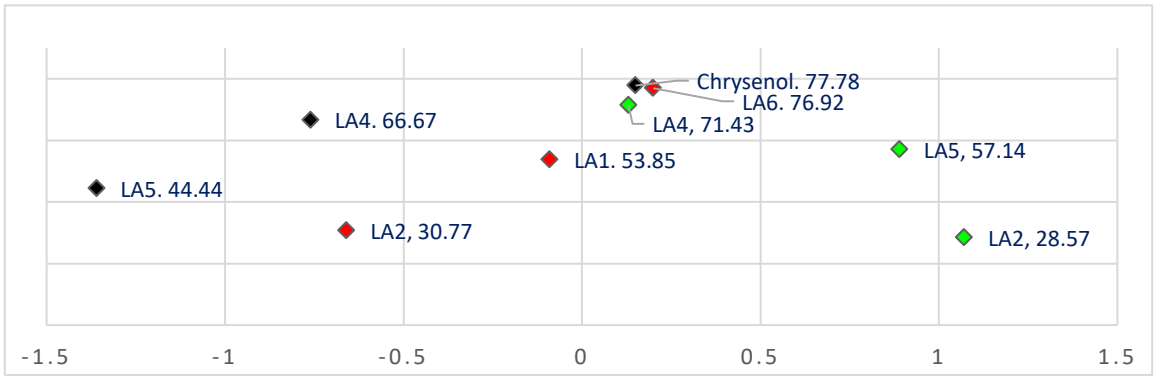

Figure 5. Residue similarity (%) between native and test ligands across CDK2, GSK-3β, and PDGFRA binding pockets: CDK2 (red diamonds), GSK-3β (green diamonds), and PDGFRA (black diamonds).

ADME and Toxicity Profiles

ADME profiling revealed that all test ligands demonstrated moderate Caco-2 permeability, supporting oral absorption potential. Chrysenol and LA3 exhibited higher human intestinal absorption values, while LA6 showed lower

absorption but favorable distribution with a high volume of distribution (1.834 L/kg). Plasma protein binding was highest for Chrysenol (97.678%) and LA2 (97.057%), indicating strong plasma retention, whereas LA6 had lower binding (78.262%), suggesting greater free drug availability. BBB penetration was predicted for LA2 and LA6, highlighting possible CNS exposure. Metabolic profiling indicated minimal CYP450 inhibition for Chrysenol, while LA4 and LA5 showed stronger inhibition risks. Excretion analysis revealed rapid clearance for LA2 (16.916 mL/min/kg), whereas Chrysenol and LA1 demonstrated moderate clearance, consistent with stable plasma retention. Collectively, these ADME and toxicity profiles suggest that Chrysenol and LA6 possess favorable drug-likeness properties, with balanced absorption, distribution, and safety, supporting their potential as lead candidates for prostate cancer inhibition. The pharmacokinetic profiles, including the predicted ADME properties of *L. aestuans* compounds and their corresponding toxicity levels, are comprehensively summarized in **Table 4** and **Table 5**, respectively.

Table 4. Predicted ADME properties of *L. aestuans* compounds

Comp.	Caco-2	Pgp I	Pgp S	HIA	PPB%	VD (L/kg)	BBB	CYP1A2 I/S	CYP2C9 I/S	CYP3A4 I/S	T½ (h)	CL (mL/min/kg)
Chry	-4.775	0.167	0.500	0.333	97.678	1.111	0.333	1/0.333	0.833/ 0.167	0.667/ 0.333	0.156	10.007
LA1	-4.714	0.167	0.333	0.167	92.075	0.472	0.333	0.167/1	0.333/ 0.833	0.833/ 0.833	0.802	11.168
LA2	-4.898	0.333	0.167	0.167	97.057	1.161	1	0.167/ 0.500	0.333/ 0.333	0.667/ 0.333	0.015	16.916
LA3	-4.964	0.167	0.167	0.333	93.406	1.032	0.500	0.167/ 0.333	0.167/ 0.167	0.333/ 0.333	0.060	9.453
LA4	-4.883	0.167	0.333	0.167	92.093	0.703	0.167	1/1	0.833/ 0.833	0.667/ 0.333	0.831	7.680
LA5	-4.727	0.167	0.167	0.167	87.572	1.932	0.833	1/1	0.333/ 0.667	0.333/ 0.667	0.889	14.946
LA6	-4.893	1	1	0.167	78.262	1.834	1	0.333/1	0.167/ 0.833	0.167/ 0.833	0.225	8.893

Toxicity profiling revealed that none of the test ligands violated acute toxicity rules. Chrysenol and LA6 exhibited three genotoxic alerts, while LA1, LA4, and LA5 showed multiple skin irritation alerts, indicating potential dermatological risks. hERG inhibition analysis suggested cardiotoxicity concerns for LA5 (0.833) and LA6 (0.500), whereas other ligands demonstrated lower values. Hepatotoxicity predictions were highest for LA1 (0.667), while AMES mutagenicity tests flagged Chrysenol (1), LA6 (0.833), and LA4 (0.667) as potential mutagens. LD_{50} values indicated that LA2 (7.012 mg/kg) and LA6 (6.165 mg/kg) were the least toxic, whereas LA1 (4.078 mg/kg) was the most toxic. Collectively, these findings suggest that although Chrysenol and LA6 show promising ADME profiles, their genotoxic and mutagenic alerts warrant further experimental validation before clinical consideration.

Table 5. Predicted toxicity profiles of *L. aestuans* compounds

Compound	Acute Toxicity Rule	Genotoxic Alerts	Skin Irritation Alerts	hERG	H-HT	AMES	LD_{50} (mg/kg)
Chrysenol	None	3 Alerts	1 Alert	0.333	0.167	1	5.367
LA1	None	None	6 Alerts	0.167	0.667	0.167	4.078
LA2	None	None	None	0.167	0.333	0.167	7.012
LA3	None	None	None	0.167	0.333	0.167	5.015
LA4	None	None	8 Alerts	0.167	0.167	0.667	5.070
LA5	None	None	5 Alerts	0.833	0.333	0.167	5.883
LA6	None	3 Alerts	2 Alerts	0.500	0.333	0.833	6.165

Limitation

Despite the promising results obtained through molecular docking and ADME-Toxicity predictions, this study has several limitations. First, the findings are based entirely on *in silico* simulations, which may not fully replicate the complex physiological conditions of a living organism. Second, while the ADME properties (**Table 4**) and toxicity profiles (**Table 5**) provide a theoretical framework for the safety and efficacy of *L. aestuans* compounds, further *in vitro* and *in vivo* experimental validations are required to confirm these biological activities and to determine the precise therapeutic dosage. Future research should focus on isolating these bioactive compounds and testing them against specific cancer cell lines to validate their potential as CDK2, GSK-3β, and PDGFRA inhibitors.

CONCLUSION

This study identified seven bioactive compounds from *L. aestuans* with therapeutic relevance against prostate cancer targets CDK2, GSK-3β, and PDGFRA. Molecular docking highlighted LA6 and Chrysenol as the most promising inhibitors, supported by favorable pharmacokinetic properties. ADME profiling suggested good oral absorption and distribution, while toxicity predictions indicated potential mutagenicity and hepatotoxicity risks that warrant further evaluation. Taken together, these findings provide novel computational evidence for *L. aestuans* derivatives as lead candidates for prostate cancer therapy. Nevertheless, further in vitro and in vivo studies are required to confirm efficacy, optimize pharmacokinetic properties, and ensure safety for clinical development.

FUNDING

The authors declare that no direct or indirect funding was received from any organization for the submitted work, and this research was conducted using independent resources.

ACKNOWLEDGMENTS

The author expresses sincere gratitude to the academic supervisors and examination committee of the Master Program in Pharmaceutical Sciences, Faculty of Pharmacy, Universitas Setia Budi, for their invaluable guidance, support, and feedback throughout the research process. The author also acknowledges the developers of ADMETlab and other open-access platforms that enabled the computational analyses conducted in this study. Thanks are due to fellow colleagues for their constructive discussions and collaborative spirit, which greatly enriched the research experience.

GENERATIVE AI DISCLOSURE STATEMENT

The authors utilized Gemini (Google) and Microsoft Copilot to assist in drafting the introduction, developing the study limitations, and refining the scientific language throughout the manuscript. Every part of the generated text was critically reviewed and edited by the authors, who take full responsibility for the content of the manuscript.

AUTHOR CONTRIBUTION STATEMENT

I Wayan Surya Rahadi: Conceptualization, Methodology, Validation, Formal Analysis, Investigation, Resources, Data Curation, Writing – Original Draft, Writing – Review & Editing, Visualization, Project Administration; **Rina Herowati**: Supervision, Validation, Writing – Review & Editing, Resources.

CONFLICT OF INTEREST

The author declares no conflict of interest related to the design, execution, or publication of this research. All analyses were conducted independently, and no financial or personal relationships influenced the outcomes or interpretations presented in this study.

REFERENCES

1. National Cancer Institute. Understanding Cancer [Internet]. 2015 [cited 2020 Oct 10]. Available from: https://www.cancer.gov/about-cancer/understanding/what-is-cancer
2. End Cancer As We Know It. Accessed April 28, 2026. https://www.cancer.org
3. Khan GJ, Khan MA, Khan T, et al. Pharmacological effects and potential therapeutic targets of DT-13. Biomed Pharmacother. 2018;97:255–63. doi:10.1016/j.biopha.2017.10.101
4. Shorning BY, Dass MS, Smalley MJ, Pearson HB. The PI3K-AKT-mTOR Pathway and Prostate Cancer: At the Crossroads of AR, MAPK, and WNT Signaling. *Int J Mol Sci*. 2020;21(12):4507. doi:10.3390/ijms21124507
5. Hare SH, Harvey AJ. mTOR function and therapeutic targeting in breast cancer. *Am J Cancer Res*. 2017;7(3):383-404.
6. Aladesanmi AJ, Famuyiwa FG, Oriola AO, Oguntimehin SA, Aiyedun PO, Arthur G. Cytotoxic Activity of Selected Nigerian Medicinal Plants. *J Herbs Spices Med Plants*. 2020;26(2):203-217. doi:10.1080/10496475.2019.1706214
7. Prostate Cancer. CancerQuest. Accessed April 29, 2026. https://cancerquest.org/patients/cancer-type/prostate-cancer

8. USDA Plants Database Plant Profile General. Accessed April 28, 2026. https://plants.sc.egov.usda.gov/plant-profile/LAAE
9. Sc O, Cs C, Nwaokezi C. Antioxidant enzyme activities and chemopreventive potentials of Laportea aestuans on urinary inflammatory markers using albino rats. Published online January 1, 2017:288-291.
10. Cao Z, Kyprianou N. Mechanisms navigating the TGF-β pathway in prostate cancer. *Asian J Urol*. 2015;2(1):11-18. doi:10.1016/j.ajur.2015.04.011
11. Liu Z, Guo F, Wang Y, et al. BATMAN-TCM: a Bioinformatics Analysis Tool for Molecular mechANism of Traditional Chinese Medicine. *Sci Rep*. 2016;6(1):21146. doi:10.1038/srep21146
12. Xie F, Ding X, Zhang QY. An update on the role of intestinal cytochrome P450 enzymes in drug disposition. *Acta Pharm Sin B*. 2016;6(5):374-383. doi:10.1016/j.apsb.2016.07.012
13. Zhang X, Zhou H, Su Y. Targeting truncated RXRα for cancer therapy. *Acta Biochim Biophys Sin*. 2016;48(1):49-59. doi:10.1093/abbs/gmv104
14. Naimi A, Soltan M, Amjadi E, Goli P, Kefayat A. Androgen Receptor Expression and Its Correlation with Clinicopathological Parameters in Iranian Patients with Triple Negative Breast Cancer. *Iran J Pathol*. 2020;15(3):239-244. doi:10.30699/ijp.2020.112819.2224
15. Goldman J, Eckhardt SG, Borad MJ, et al. Phase I dose-escalation trial of the oral investigational Hedgehog signaling pathway inhibitor TAK-441 in patients with advanced solid tumors. *Clin Cancer Res Off J Am Assoc Cancer Res*. 2015;21(5):1002-1009. doi:10.1158/1078-0432.CCR-14-1234
16. Dietrich C, Trub A, Ahn A, et al. INX-315, a Selective CDK2 Inhibitor, Induces Cell Cycle Arrest and Senescence in Solid Tumors. *Cancer Discov*. 2024;14(3):446-467. doi:10.1158/2159-8290.CD-23-0954
17. Knudsen ES, Witkiewicz AK, Sanidas I, Rubin SM. Targeting CDK2 for cancer therapy. *Cell Rep*. 2025;44(8):116140. doi:10.1016/j.celrep.2025.116140
18. Liang J, Pan Y, Yang J, Zeng D, Li J. WNT signaling in cancer: molecular mechanisms and potential therapies. *Mol Biomed*. 2025;6:83. doi:10.1186/s43556-025-00327-x
19. Reddy SK, Reddy SVG, Basha SH. Discovery of novel PDGFR inhibitors targeting non-small cell lung cancer using a multistep machine learning assisted hybrid virtual screening approach. *RSC Adv*. 2025;15(2):851-869. doi:10.1039/D4RA06975G
20. El-Hachem N, Haibe-Kains B, Khalil A, Kobeissy FH, Nemer G. AutoDock and AutoDockTools for Protein-Ligand Docking: Beta-Site Amyloid Precursor Protein Cleaving Enzyme 1(BACE1) as a Case Study. *Methods Mol Biol*. 2017;1598:391-403. doi:10.1007/978-1-4939-6952-4_20
21. Forli S, Huey R, Pique ME, Sanner MF, Goodsell DS, Olson AJ. Computational protein-ligand docking and virtual drug screening with the AutoDock suite. *Nat Protoc*. 2016;11(5):905-919. doi:10.1038/nprot.2016.051
22. (PDF) SAWAR OTAK. *ResearchGate*. Published online January 5, 2026. doi:10.29342/cnj.v2i1.54
23. Persidsky Y, Ramirez SH, Haorah J, Kanmogne GD. Blood-brain barrier: structural components and function under physiologic and pathologic conditions. *J Neuroimmune Pharmacol Off J Soc NeuroImmune Pharmacol*. 2006;1(3):223-236. doi:10.1007/s11481-006-9025-3
24. Acikgoz E, Ozdil B, Oktem G, Aktug H, Ragbetli MC, Tas C. GSK-3 inhibitor induces apoptosis and cell cycle arrest in CD133+/CD44+ prostate cancer cells through modulation of Notch signaling pathway. *Mol Biol Rep*. 2025;52(1):892. doi:10.1007/s11033-025-10977-3
25. Hua L, Anjum F, Shafie A, et al. Identifying promising GSK3β inhibitors for cancer management: a computational pipeline combining virtual screening and molecular dynamics simulations. *Front Chem*. 2023;11. doi:10.3389/fchem.2023.1200490
26. Siskin M, Economides MP, Wise DR. Cyclin-Dependent Kinase Inhibition in Prostate Cancer: Past, Present, and Future. *Cancers*. 2025;17(5):774. doi:10.3390/cancers17050774
27. Shiota M, Fujimoto N, Kashiwagi E, Eto M. The Role of Nuclear Receptors in Prostate Cancer. *Cells*. 2019;8(6):602. doi:10.3390/cells8060602
28. Mayr L, Neyazi S, Schwark K, et al. Effective targeting of PDGFRA-altered high-grade glioma with avapritinib. *Cancer Cell*. 2025;43(4):740-756.e8. doi:10.1016/j.ccell.2025.02.018
29. Zhang R, Yao Y, Gao H, Hu X. Mechanisms of angiogenesis in tumour. *Front Oncol*. 2024;14. doi:10.3389/fonc.2024.1359069
30. Zheng Y, Trivedi T, Lin RC, et al. Loss of the vitamin D receptor in human breast and prostate cancers strongly induces cell apoptosis through downregulation of Wnt/β-catenin signaling. *Bone Res*. 2017;5(1):17023. doi:10.1038/boneres.2017.23